LASER
& PHOTONICS
REVIEWS

Supporting Information

for *Laser Photonics Rev.*, DOI 10.1002/lpor.202401114

Chiral Bulk Solitons in Photonic Graphene with Decorated Boundaries

Shuang Shen, Ce Shang, Yongdong Li and Yiqi Zhang**

Supplemental Materials *of*
Chiral bulk solitons in photonic graphene with decorated boundaries

Shuang Shen,[1] Ce Shang,[2,*] Yongdong Li,[1] and Yiqi Zhang[1,†]

[1] *Key Laboratory for Physical Electronics and Devices, Ministry of Education, School of Electronic Science and Engineering, Xi'an Jiaotong University, Xi'an 710049, China*

[2] *Aerospace Information Research Institute, Chinese Academy of Sciences, Beijing 100094, China*

I. CONFIGURATION AND BAND STRUCTURE FOR DARK SOLITONS

Contrary to the lattice shown in Fig. 1(b) in the main text, we can also make the depth of the outermost sites of the honeycomb ribbon deeper than that of the other sites, as shown in Fig. S1(b). The lattice depth is $\boldsymbol{p} = (8, 10)$. The corresponding band structure is displayed in Fig. S1(a), in which the red curve represents the chiral bulk state.

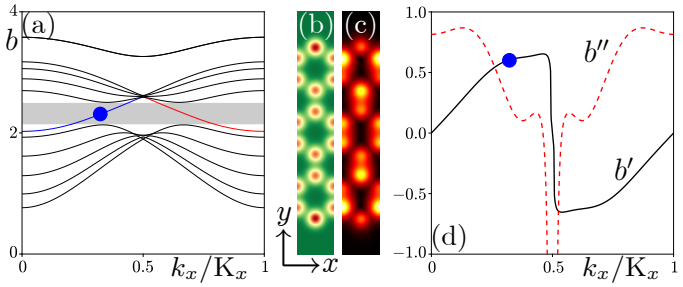

FIG. S1. (a) Band structure of the honeycomb lattice ribbon with 12 sites in the supercell. The blue and red curves represent the chiral bulk states. The shaded region represents the band gap. (b) Honeycomb supercell. The upper and bottom sites are deeper than other sites. (c) Field module distribution of the chiral bulk state at $k_x = 0.30\mathrm{K}_x$ that corresponds to the blue dot. (d) First-order b' (black solid curve) and second-order b'' (red dashed curves) derivatives of the chiral bulk state. Panels in (b,c) are shown in the window $0 \le x \le \sqrt{3}a$ and $-8 \le y \le 8$.

The chiral bulk state is still in the band gap, but its property is different from that of the chiral bulk state in Fig. 1(a) in the main text. We choose one chiral bulk state and show its field modulus profile in Fig. S1(c). The energy of the state at the outermost sites is not the strongest, which is different from the chiral bulk state in Fig. 1(c) in the main text. According to the first-order (b') and second-order (b'') derivatives of the chiral bulk state shown in Fig. S1(d), it is natural to conclude that the chiral bulk state in this configuration in Fig. S1(b) is only ready for generating dark chiral bulk solitons, since b'' is almost positive in the first Brillouin zone,

II. DARK CHIRAL BULK SOLITONS

Similar to the bright chiral bulk solitons in the main text, the dark chiral bulk solitons can be prepared by superimposing the dark soliton envelope to the linear chiral bulk state. The dark envelope is written as

$$\mathcal{A}(x,z) = \sqrt{\frac{b_{\mathrm{nl}}}{\chi}}\tanh\left(\sqrt{\frac{b_{\mathrm{nl}}}{b''}}\left(x + b'z\right)\right)\exp\left(ib_{\mathrm{nl}}z\right), \tag{S1}$$

and the field modulus profile of the dark chiral bulk soliton is displayed in Fig. S2(a). Since the first-order derivative is positive, the dark soliton moves in negative x direction, as shown by the white arrow in Fig. S2(a). One finds the dark chiral bulk soliton does not change its profile during propagation, as indicated by the field modulus profiles at

* shangce@aircas.ac.cn
† zhangyiqi@xjtu.edu.cn

selective distances in Fig. S2(a). The linear propagation of the dark chiral bulk soliton is also investigated, and the field modulus profile at $z = 1000$ is shown in Fig. S2(b). Clearly, the dark notches in Fig. S2(b) are wider than those in Fig. S2(a), which is a reflection of broadening due to the diffraction.

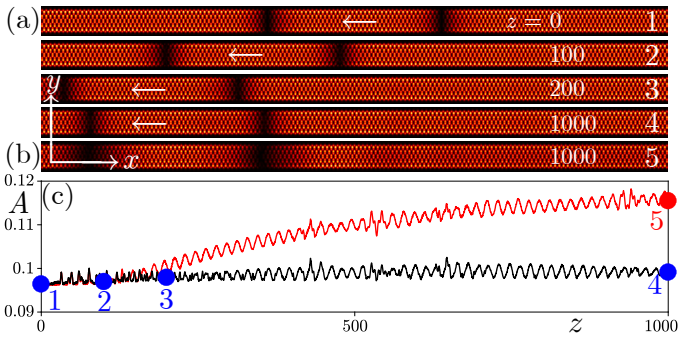

FIG. S2. (a) Amplitude modulus profiles of the chiral bulk soliton at typical distances corresponding to the dots $1 \sim 4$ in (c). The arrow indicates the moving direction of the soliton. (b) Amplitude modulus profile of the soliton at $z = 1000$ after linear propagation corresponding to the dot 5 in (c). (c) Peak amplitude of the soliton during propagation. The black curve is for the nonlinear propagation, while the red curve records the linear propagation. Parameters are $b_{\rm nl} = 0.003$, $k_x = 0.30\mathrm{K}_x$, $b' = 0.5880$, $b'' = 0.3440$ and $\chi = 0.0803$. Panels in (a,b) are shown in the window $-180 \le x \le 180$ and $-8 \le y \le 8$.

The peak amplitudes of the dark chiral bulk soliton during nonlinear propagation and linear propagation are shown in Fig. S2(c), as indicated by the black curve and red curve, respectively. Even though the black curve exhibits an oscillating behavior versus propagation distance z, it does not show explicitly decaying or increasing. However, the red curve increases with the propagation distance, which is distinct from the black curve, and demonstrates the formation of dark chiral bulk solitons in this configuration.

III. ESTABLISHMENT OF THE CHIRAL BULK SOLITON WITH INCREASING POWER

As shown in Fig. 4(a) in the main text, the chiral bulk soliton is thresholdless, so one can always construct a soliton with a certain power (corresponding to a fixed $b_{\rm nl}$). In other words, if the value of $b_{\rm nl}$ is given, one can only obtain the soliton with a certain power, with which the self-trapping from the nonlinearity will balance the diffraction. To see the establishment of the chiral bulk soliton, we choose the soliton in Fig. 4(d) in the main text as an example. We multiply a factor within $[0, 1]$ to it and do propagation to $z = 1000$ and see its field modulus profile, as shown in Fig. S3. The field modulus profile in Fig. S3(a) shows the initial localized wavepacket that is same as that in Fig. 4(d) in the main text. When the nonlinearity is lifted, the wavepacket will not show diffraction during propagation, as shown in Fig. S3(b), which is same as that in Fig. 4(e) in the main text. For the nonlinear propagation, the diffraction is prohibited a bit if the initial wavepacket $\psi(x, y)$ is multiplied with 0.5 as shown in Fig. S3(c). If the factor becomes 0.8, the role of the nonlinearity is strengthened, and the beam width decreases further, as shown in Fig. S3(d). The case in Fig. S3(e) that is same as that in Fig. 4(d) in the main text, shows the balance between the nonlinearity and the diffraction, and one obtains the soliton.

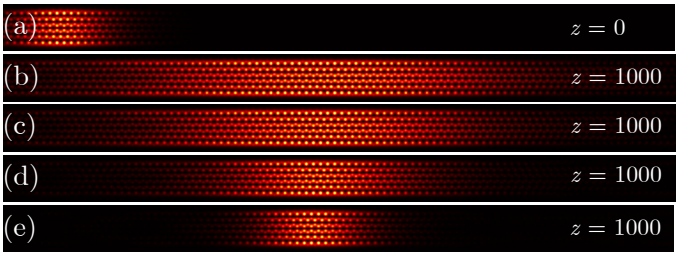

FIG. S3. (a) The initial localized wavepacket $\psi(x, y)$ that is same as that in Fig. 4(d) in the main text. (b) Linear propagation of the initial wavepacket at $z = 1000$ that is same as that in Fig. 4(e). (c)-(d) Nonlinear propagation of the initial wavepacket at $z = 1000$ with the input $\psi(x, y)$ multiplied a factor 0.5, 0.8, and 1.0, respectively. The case in (e) is same as that in Fig. 4(d) in the main text and is a soliton since the diffraction is balanced with the self-trapping effect of the nonlinearity. Parameters are $k_x = 0.30\mathrm{K}_x$, $b' = 0.5880$, $b'' = 0.3440$ and $\chi = 0.0803$. Panels are shown in the window $-115 \le x \le 115$ and $-8 \le y \le 8$.

IV. UNSTABLE BRIGHT SOLITONS WITH NOISE

The chiral bulk solitons may either be stable or unstable are indicated by the solid line and dashed line in Fig. 4(a) in the main text. As stated in the main text, we superimpose a random noise to the chiral bulk soliton and do propagation over a long distance. If the soliton is stable, its peak amplitude and profile do not change during propagation. While for the unstable soliton, its peak amplitude will oscillate in a chaotic-like behavior and its field modulus profile does not hold. In Fig. S4, we display the peak amplitude and the field modulus profiles at selective distances. Indeed, the unstable soliton cannot hold its original landscape during propagation.

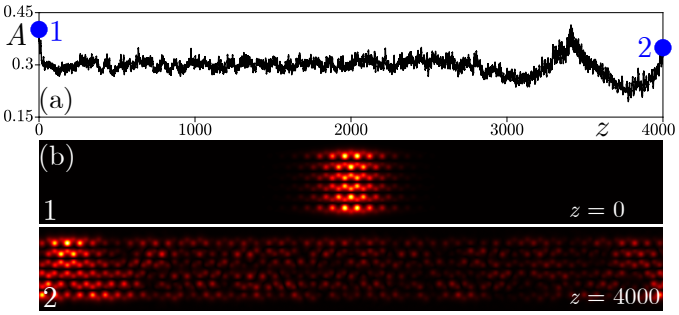

FIG. S4. (a) Peak amplitude of the unstable chiral bulk soliton with $b_{\rm nl} = 0.027$ superposed with a random noise. (b) Amplitude modulus profiles of the chiral bulk soliton at typical distances corresponding to the dots 1 and 2 in (a). Other parameters are $k_x = 0.30\mathrm{K}_x$, $b' = 0.5880$, $b'' = 0.3440$ and $\chi = 0.0803$. Panels in (b) are shown in the window $-60 \leq x \leq 60$ and $-8 \leq y \leq 8$.